

Multi-View Vision-to-Geometry Knowledge Transfer for 3D Point Cloud Shape Analysis

Qijian Zhang, Junhui Hou, *Senior Member, IEEE*, and Yue Qian

Abstract—As two fundamental representation modalities of 3D objects, 2D multi-view images and 3D point clouds reflect shape information from different aspects of visual appearances and geometric structures. Unlike deep learning-based 2D multi-view image modeling, which demonstrates leading performances in various 3D shape analysis tasks, 3D point cloud-based geometric modeling still suffers from insufficient learning capacity. In this paper, we innovatively construct a unified cross-modal knowledge transfer framework, which distills discriminative visual descriptors of 2D images into geometric descriptors of 3D point clouds. Technically, under a classic teacher-student learning paradigm, we propose multi-view vision-to-geometry distillation, consisting of a deep 2D image encoder as teacher and a deep 3D point cloud encoder as student. To achieve heterogeneous feature alignment, we further propose visibility-aware feature projection, through which per-point embeddings can be aggregated into multi-view geometric descriptors. Extensive experiments on 3D shape classification, part segmentation, and unsupervised learning validate the superiority of our method. We will make the code and data publicly available.

Index Terms—3D point cloud, multi-view 2D image, knowledge transfer, cross-modal distillation, 3D shape analysis

1 INTRODUCTION

DRIVEN by the recent advancements in 3D data acquisition and perception, deep learning-based 3D shape analysis is attracting increasingly growing attention in both industrial and academia. Depending on different representation modalities of 3D shape models, mainstream learning paradigms can be categorized into: 1) image-based [1], [2], [3], [4], [5], 2) voxel-based [6], [7], [8], [9], [10], and 3) point-based [11], [12], [13], [14], [15]. Currently, there is no unified modeling paradigm for 3D shape understanding, as each method uniquely has different merits and limitations.

Image-based methods represent 3D models by a collection of multi-view 2D images rendered from multiple viewpoints. Benefiting from advanced image modeling architectures [16], [17], [18], [19] and large-scale richly-annotated image databases [20], [21], [22], [23], [24], multi-view learning has demonstrated dominating performance in various shape recognition tasks [2], [25], [26]. However, shape rendering is performed on high-quality man-made polygon meshes, which are not directly available from real-world sensors/scanners, and inevitably lose interior geometric structure and detailed spatial texture. *Voxel-based* methods employ volumetric grids to depict spatial occupancy of 3D models, such that standard 3D convolutional architectures can be naturally extended for feature extraction without additional efforts to develop specialized learning operators. Unfortunately, due to the cubic growth of computational complexity and memory footprint, this learning paradigm is more suitable for dealing with low-resolution volumes, and complicated hierarchical 3D indexing structure [8], [9], [10] with careful configuration is required for processing denser voxels and capturing geometric details. In recent years, *point-based* methods that directly operate on unstructured

3D point clouds without any pre-processing procedures gradually gain popularity. As the most straightforward geometry representation modality, point clouds serve as raw outputs of many 3D acquisition devices and faithful record of spatial information. However, different from images/voxels defined on regular grids, point clouds are characterized by irregularity and unorderedness, which cause great difficulties in feature abstraction. Consequently, there still exists a lot of room for further performance enhancement in point-based learning frameworks.

Motivated by the complementary properties between *image-based visual modeling* and *point-based geometric modeling*, this paper explores the possibility of transferring knowledge extracted from powerful deep image encoders into deep point encoders for boosting downstream shape analysis performance. Technically, we innovatively propose multi-view vision-to-geometry distillation (MV-V2GD), a unified processing pipeline following a standard teacher-student architecture design for cross-modal knowledge transfer. As illustrated in Fig. 1, given a 3D shape, we feed a collection of multi-view 2D images into a pretrained deep 2D image encoder in the teacher branch to produce multi-view visual descriptors, while in the student branch we feed a 3D point cloud into a deep point encoder to produce high-dimensional per-point embeddings. Under the same camera poses, we compute point-wise view-specific visibility, based on which we produce multi-view geometric descriptors. By performing feature alignment between multi-view visual and geometric descriptors, the student model can be guided to learn more discriminative point-wise features for geometric shape understanding. To verify the effectiveness of the proposed MV-V2GD framework, we select common deep point encoders [11], [12], [15] as baseline student models, and conduct experiments on three benchmark tasks, including shape classification, part segmentation, and unsupervised learning, where we achieve obvious and stable

- Q. Zhang, J. Hou, and Y. Qian are with the Department of Computer Science, City University of Hong Kong, Hong Kong SAR. Email: qijizhang3-c@my.cityu.edu.hk; jh.hou@cityu.edu.hk; yueqian4-c@my.cityu.edu.hk;

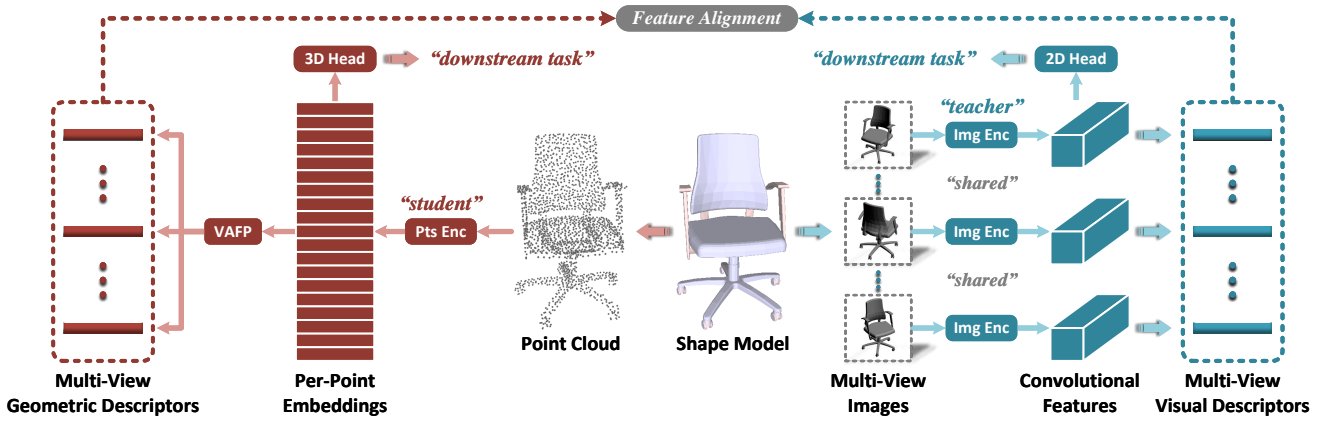


Fig. 1. Overall flowchart of the proposed MV-V2GD cross-modal knowledge transfer framework, which involves a pretrained image-based teacher branch (right) and a point-based student branch (left) to be distilled by multi-view feature alignment. The whole teacher branch is fixed in the training phase to provide discriminative knowledge, and removed in the testing phase such that we make inference solely from point clouds.

performance gains.

In summary, the main contributions of this paper are three-fold:

- We present a unified MV-V2GD learning framework, which makes *the first* attempt to transfer knowledge from multi-view 2D visual modeling to 3D geometric modeling for 3D point cloud shape analysis.
- To facilitate multi-view visual-geometric feature alignment, we particularly develop a simple yet effective VAFP mechanism that aggregates per-point embeddings into view-specific geometric descriptors.
- We observe highly encouraging performance improvement on a rich variety of downstream tasks and baseline models, which reveals a new and generic paradigm for enhancing the learning capacity of point cloud networks.

The remainder of this paper is organized as follows. In Sec. 2, we discuss closely related studies on multi-view 3D shape analysis, deep set architectures, and 2D-3D knowledge transfer. In Sec. 3, we start by summarizing the working mechanism of our proposed method in Sec. 3.1 and presenting general formulations of mainstream deep 2D image and 3D point encoders in Sec. 3.2 and Sec. 3.3, respectively, based on which we construct a unified multi-view cross-modal feature alignment scheme in Sec. 3.4 and then introduce a novel visibility-aware feature projection (VAFP) mechanism, which can elegantly produce view-specific pairs of visual-geometric representation. Finally, we summarize the overall training objective and strategy in Sec. 3.5. In Sec. 4, we report experimental results on different baseline deep point encoders and benchmark tasks. Finally, we present some critical discussions in Sec. 5 and conclude the whole paper in Sec. 6.

2 RELATED WORK

Multi-View 3D Shape Analysis. As a natural extension of 2D deep learning, multi-view 3D shape modeling is typically built upon various variants of multi-input 2D convolutional neural networks (CNNs). Pioneered by MVCNN [1] that separately consumes multi-view images rendered from pre-defined camera poses and generates

global shape signature by cross-view max-pooling, many follow-up works are devoted to designing more advanced view aggregation and/or selection strategies. GVCNN [27] constructs a three-level hierarchical correlation modeling framework that adaptively groups multi-view descriptors into different clusters. MHBN [3] and RelationNet [28] further exploit patch-level interaction to enrich inter-view relationships. RotationNet [4] treats viewpoint indices as learnable latent variables and proposes to jointly estimate object pose and category. EMV [29] presents a group convolution approach that operates on a discrete subgroup of rotation groups to extract rotation-equivalent shape descriptors. More recently, View-GCN [5] treats multiple views as graph nodes to form the corresponding view graph, on which graph convolution is applied to learn multi-view relations. MVTN [30] adaptively regresses optimal viewpoints by introducing differentiable rendering, which enables end-to-end training.

Deep Learning on 3D Point Clouds. Pioneered by PointNet [11] that adopts point-wise multi-layer perceptrons (MLPs) to achieve permutation-invariant feature extraction, deep set architectures that directly operate on point clouds for 3D geometric modeling have rapidly gained popularity. Inheriting the successful design paradigm of deep CNNs, PointNet++ [12] introduces local neighborhood aggregation and employs progressive downsampling for hierarchical abstraction. A rich variety of highly-specialized point convolution operators have been investigated in later works. [31], [13], [32], [14], [33] mimic standard convolutions by learning adaptive weights for kernel matching. [34], [35], [36], [37], [38] conduct more complicated point feature aggregation strategies to enhance network capacity. DGCNN [15] present a graph-based dynamic feature updating mechanism, which enables to capture global contextual information. [39], [40], [41] explore learning-based, instead of heuristic, subset selection techniques. Very recently, transformer architectures [42], [43], [44], [45], [46], [47] are also adapted for point cloud modeling.

Cross-Modal Knowledge Transfer between 2D and 3D. As pointed out in [48], despite the proliferation of knowledge

distillation studies, there is relatively little effort on cross-modal scenarios with obvious modality gaps due to the lack of paired samples, and this task becomes even more challenging when conducted between 2D and 3D domains. xMUDA [49] proposes to implement unsupervised domain adaptation from source domain of single-view images and target domain of point clouds by aligning 2D and 3D outputs based on pixel-point correspondences. PPKT [50] constructs a 3D pretraining pipeline that applies contrastive learning strategy on positive and negative pixel-point pairs, in order to leverage 2D pretrained knowledge. In an opposite transfer direction, Pri3D [51] explores the potential of 3D-guided contrastive pretraining for boosting 2D perception. In addition to maintaining feature consistency between paired 2D pixels and 3D points, this work also aims to learn invariant pixel descriptors across image scans captured from different viewpoints. A more flexible and 3D-to-2D distillation framework can be found in [52], which aligns statistical distributions of 2D and 3D CNN features through specialized dimension normalization. Particularly, to get rid of the dependence on fine-grained correspondence between 2D and 3D modalities that are typically expensive to acquire, this work additionally explores a semantic-aware adversarial training scheme to deal with unpaired 2D images and 3D volumetric grids. Generally, existing works mainly focus on scene-level understanding, due to the availability of correspondence information between 2D and 3D data. Currently, to the best of our knowledge, there is no previous study on cross-modal knowledge transfer for shape analysis tasks.

3 PROPOSED METHOD

3.1 Problem Overview

We consider two complementary learning paradigms for 3D shape understanding, i.e., 2D visual modeling driven by 2D multi-view images, and 3D geometric modeling driven by 3D point clouds. As afore-mentioned, owing to the regular data structure and powerful learning architecture, image-based deep models can extract discriminative feature representations, despite the loss of partial geometric information. Comparatively, although 3D point clouds preserve complete 3D geometry, their structural irregularity causes great challenges in feature extraction, and thus point-based deep models suffer from relatively insufficient learning capacity. Hence, our goal is to distill the discriminative knowledge extracted from a deep 2D image encoder into a deep 3D point encoder, which is actually a rather challenging problem due to significant domain gaps in terms of both network architecture and data modality.

Formally, given a 3D model, let $\mathcal{P} \in \mathbb{R}^{N \times 3}$ be its 3D point cloud representation with N points, and $\{\mathcal{I}_k \in \mathbb{R}^{H \times W \times 3}\}_{k=1}^K$ a collection of 2D multi-view images $\{\mathcal{I}_k \in \mathbb{R}^{H \times W \times 3}\}_{k=1}^K$ that depict its view-specific visual appearance when rendered from K virtual camera positions $\{\mathbf{c}_k = (\theta_k^{az}, \theta_k^{el}, \mu)\}_{k=1}^K$, where θ_k^{az} and θ_k^{el} denote azimuth and elevation angles relative to the centroid at viewpoint \mathbf{c}_k , and μ is specified as a constant observation distance.

Following the conventional teacher-student architecture design in the field of knowledge distillation [53], the proposed MV-V2GD learning framework consists of a 2D

teacher branch $\mathcal{B}_t = \{\mathcal{M}_t, \mathcal{H}_t\}$ and a 3D student branch $\mathcal{B}_s = \{\mathcal{M}_s, \mathcal{H}_s\}$, in which \mathcal{M}_t represents a deep 2D image encoder, \mathcal{M}_s represents a deep 3D point encoder to be distilled, \mathcal{H}_t and \mathcal{H}_s represent the corresponding task-specific head networks. Generally, the overall processing pipeline of is composed of three sequential stages:

- 1) Pretraining the teacher branch \mathcal{B}_t on 2D multi-view images.
- 2) Training the student branch \mathcal{B}_s on 3D point clouds while in the meantime transferring knowledge exported from fixed \mathcal{M}_t into \mathcal{M}_s through multi-view visual-geometric feature alignment.
- 3) Deploying the distilled student branch \mathcal{B}_s , in the *testing* phase, to make inference solely from 3D point clouds.

Our working mechanism is fundamentally different from multi-modal fusion, in which data of multi-modalities are consumed as inputs at both training and testing phases. Functionally, we emphasize that MV-V2GD serves as a universal learning paradigm that can be seamlessly applied to generic deep point encoders for enhancing network capacity.

3.2 Teacher Network for 2D Image Modeling

Deep convolutional architectures have demonstrated the remarkable ability to learn discriminative visual features from 2D images. Benefiting from the proliferation of mature 2D CNN backbone networks pretrained on large-scale image databases [22], we can always conveniently select an appropriate and powerful off-the-shelf deep 2D image encoder as our 2D teacher model \mathcal{M}_t , which separately consumes multi-view images as inputs and correspondingly produce high-dimensional convolutional feature maps. Formally, we can formulate a general description of the teacher model behaviors as

$$\{\mathcal{V}_k\}_{k=1}^K = \mathcal{M}_t \left(\{\mathcal{I}_k\}_{k=1}^K \right), \quad (1)$$

where $\mathcal{V}_k \in \mathbb{R}^{H' \times W' \times C_t}$ denotes a view-specific 2D feature map extracted from shape rendering \mathcal{I}_k , which partially encodes visual patterns of the original 3D model when observed from viewpoint \mathbf{c}_k .

After backbone feature extraction, we apply global average pooling (GAP) [54] on the generated 2D convolutional feature maps, i.e., $\{\mathcal{V}_k\}_{k=1}^K$, to deduce a collection of vectorized multi-view visual descriptors $\{\mathbf{v}_k \in \mathbb{R}^{C_t}\}_{k=1}^K$, which serve as teacher knowledge to be transferred into the target student model.

3.3 Student Network for 3D Point Cloud Modeling

In contrast to mature 2D image modeling, deep learning on 3D point clouds is still a newly-emerging yet fast-growing research area. Restricted by the scarcity of large-scale shape repository and the difficulty of 3D annotation, the current deep set architectures are actually far from deep, in order to relieve parameter overfitting, and are typically trained from scratch when applied to downstream tasks. Consequently, point-based learning models demonstrate insufficient learning capacity for capturing discriminative geometric feature representations.



Fig. 2. Illustration of multi-view visibility checking. Under pre-defined camera poses, we correspondingly generate a collection of multi-view images and partial point clouds, as placed in the first and second rows. In the third row, we also provide visualizations of visible points when observed from the opposite azimuth angles.

We consider a deep 3D point encoder \mathcal{M}_s as the target 3D student model to be distilled, which consumes an irregular set of spatial points as inputs and produce high-dimensional point-wise embeddings. Without loss of generality, we can describe the student model behaviors as

$$\mathcal{G} = \mathcal{M}_s(\mathcal{P}), \quad (2)$$

where $\mathcal{G} \in \mathbb{R}^{N_a \times C_s}$ represents a set of C_s -dimensional feature vectors extracted from N input points. Taking a step forward, the actual learning process operating on \mathcal{P} can be further detailed as

$$\mathcal{M}_s(\mathcal{P}) = \varphi_{\text{bm}}(\mathcal{A}), \quad (3)$$

where $\mathcal{A} \in \mathbb{R}^{N_a \times 3}$ represents N_a what we call feature anchor points, and $\varphi_{\text{bm}}(\cdot)$ denotes a learned feature mapping that point-wisely embeds 3D anchor points in \mathcal{A} to their corresponding feature vectors in \mathcal{G} .

Practically, depending on specific network architectures and task properties, there exist different definitions and implementations of feature anchor points \mathcal{A} . In hierarchical learning frameworks ($N_a < N$), \mathcal{A} can be either a down-sampled subset of the original point cloud [12], [36], [38] or a sparser set of adaptively generated anchor positions [34], [41], [40]. By contrast, many other approaches [11], [31], [15] choose to directly deduce point-wise embeddings for all input points ($N_a = N$), which means that \mathcal{A} is totally equivalent to the input point cloud \mathcal{P} .

3.4 Multi-View Visibility-Aware Feature Alignment

Different from conventional development protocols of knowledge distillation that focus on homogeneous model architectures (e.g., deep and shallow CNNs) and/or the same data structure but different contents (e.g., RGB and depth images), here we are faced with obvious heterogeneity (i.e., 2D and 3D) of both model and data. Hence, our main concern is to reasonably establish connections between K view-specific visual descriptors $\{\mathbf{v}_k\}_{k=1}^K$ extracted from \mathcal{M}_t and N_a anchor point feature vectors contained in \mathcal{G} extracted from \mathcal{M}_s .

Intuitively, each individual \mathbf{v}_k encodes partial shape appearance visible from viewpoint \mathbf{c}_k , while \mathcal{G} captures complete shape geometry from all points. Such asymmetry motivates us to investigate a symmetric feature alignment framework based on view-specific feature projection, where we distill teacher knowledge into the student model by minimizing the following loss function

$$\mathcal{L}_{\text{dist}} = \sum_{k=1}^K \|\mathbf{v}_k - \phi_k(\mathcal{G})\|_1 \quad (4)$$

where $\phi_k(\cdot)$ denotes a learnable feature projection process that aggregates point-wise embeddings to form a vectorized geometric descriptor, i.e., $\mathbf{g}_k \in \mathbb{R}^{C_t}$, which encodes partial shape structure when observed from viewpoint \mathbf{c}_k . This enables us to conveniently align each pair of $\{\mathbf{v}_k\}_{k=1}^K$ and $\{\mathbf{g}_k\}_{k=1}^K$ to sufficiently exploit multi-view teacher knowledge in an interpretable manner.

Obviously, under our proposed knowledge transfer framework, the core problem is to design an effective view-specific geometric feature projector ϕ_k . To this end, we present a novel VAFP mechanism to generate $\{\mathbf{g}_k\}_{k=1}^K$ from \mathcal{G} according to per-point visibility of feature anchors \mathcal{A} .

Specifically, we employ a simple and fast hidden point removal algorithm [55] to determine visibility status of all N_a anchor points in \mathcal{A} when observed from pre-defined camera poses, as illustrated in Fig. 2. This geometrically meaningful selection mechanism allows us to aggregate feature anchors \mathcal{A} into K groups of visible subsets $\{\tilde{\mathcal{A}}_k \in \mathbb{R}^{N_k \times 3}\}_{k=1}^K$, in which $\tilde{\mathcal{A}}_k \subseteq \mathcal{A}$, with respect to viewpoints $\{\mathbf{c}_k\}_{k=1}^K$. In the meantime, note that anchor points in \mathcal{A} and feature embeddings in \mathcal{G} form one-to-one (i.e., row-wise) correspondence, we can directly obtain K clusters of feature vectors $\{\tilde{\mathcal{G}}_k \in \mathbb{R}^{N_k \times C_s}\}$ ($\tilde{\mathcal{G}}_k \subseteq \mathcal{G}$) that are mapped from visible anchor points $\tilde{\mathcal{A}}_k$.

After the above visible feature grouping process, we can deduce a collection of multi-view geometric descriptors $\{\mathbf{g}_k\}_{k=1}^K$ by

$$\mathbf{g}_k = \phi_k(\mathcal{G}) = \tilde{h}_{\text{align}}(\rho_{\max}(\tilde{\mathcal{G}}_k)) \quad (5)$$

where $\rho_{\max}(\cdot)$ means applying channel max-pooling on \tilde{G}_k to produce a vectorized C_s -dimensional codeword, $\tilde{h}_{\text{align}}(\cdot)$ is implemented as a single fully-connected (FC) layer that achieves channel alignment between visual and geometric descriptors. See Sec. 4.4 for verification of the superiority of our VAFP-driven knowledge transfer framework compared with conventional distillation paradigms.

3.5 Overall Objective

Given a specific 3D shape analysis task, we formulate the overall training objective $\mathcal{L}_{\text{overall}}$ as a weighted combination of the distillation loss $\mathcal{L}_{\text{dist}}$ (Eq. 4) and the corresponding task loss $\mathcal{L}_{\text{task}}$, which can be formulated as

$$\mathcal{L}_{\text{overall}} = \omega_t \cdot \mathcal{L}_{\text{task}} + \omega_d \cdot \mathcal{L}_{\text{dist}}, \quad (6)$$

where we empirically set $\omega_t = 0.1$ and $\omega_d = 1/K$ in all our experiments. Note that $\mathcal{L}_{\text{task}}$ drives the optimization of the whole student learning branch including encoder \mathcal{M}_s and head \mathcal{H}_s , while $\mathcal{L}_{\text{dist}}$ only influences encoder \mathcal{M}_s by constraining its feature outputs.

Particularly, when dealing with some types of deep point encoders (e.g., [11]) that require optimizing auxiliary regularizers, we conform to the original weighting factors applied on regularization terms without multiplying ω_t .

4 EXPERIMENTS

We evaluate the effectiveness of our proposed MV-V2GD framework in three application scenarios, i.e., shape classification (Sec. 4.1), part segmentation (Sec. 4.2), and reconstruction-driven unsupervised learning (Sec. 4.3). Within each sub-section, we introduce benchmark datasets and data preparation procedures, after which we provide main technical implementations of both teacher and student model architectures. In the end, we provide specific comparison experiments and performance analyses.

4.1 Shape Classification

Data Preparation. ModelNet40 [7] is a common 3D object dataset containing 12311 polygon mesh models covering 40 man-made categories. Following the official split, we used 9843 shapes for training and the rest 2468 for testing.

For geometric modeling, we applied classic Poisson disk sampling (PDS) to uniformly sample 1024 spatial points from mesh faces. For visual modeling, we adopted the same multi-view shape rendering pipeline as proposed in [56], where $K = 12$, $\theta_k^{az} \in \{k\pi/6\}_{k=1}^{12}$, $\theta_k^{el} = \pi/6$, $r = 1$.

Architecture of the Teacher Network. Generally, we adopted a mature multi-view learning framework (i.e., MVCNN [1]) built upon multi-input CNNs as the teacher branch \mathcal{B}_t , while conducting some modifications to both encoder \mathcal{M}_t and head \mathcal{H}_t for performance improvement. A block diagram of the overall teacher branch for image-based shape classification is illustrated in Fig. 3.

Specifically, we employed a light-weight 2D CNN backbone (i.e., MobileNetV2 [57]) to extract deep convolutional features and vectorized visual descriptors from input multi-view images. Besides, in addition to outputting the final class scores (logits) from a single

global shape signature, we tended to independently predict shape categories from all views by adding side-output supervisions.

Architecture of the Student Network. We selected three *representative* deep point cloud modeling architectures, including 1) PointNet [11], 2) PointNet++ [12], and 3) DGCNN [15], as the target student point encoders \mathcal{M}_s . Besides, we also experimented with CurveNet [58], a more recent state-of-the-art learning model. In the original implementations, the classification head \mathcal{H}_s is composed of three fully-connected layers that transform a global shape signature into category logits, while in all our experiments we uniformly simplified \mathcal{H}_s into a single linear layer. *Note that, in the testing phase, we did not employ any voting techniques [36], [33], [59], [58] that turn to be highly cumbersome and unstable.*

Quantitative Results. We listed shape classification accuracy of both the original and the distilled models in Table 1. As an earlier work with simple architecture design, PointNet officially reports overall accuracy of 89.2%, which is thought to be far from satisfactory. Surprisingly, driven by MV-V2GD, this model performs even better than the original PointNet++, which involves much more complicated learning patterns. Benefiting from strengthened modeling capacity, PointNet++ further reaches highly competitive 93.3% after distillation. DGCNN represents a common type of powerful graph-style point cloud modeling paradigm, which is boosted from 92.9% to 93.7% with obvious performance improvement of 0.8%. Even for the state-of-the-art CurveNet, our method still contributes satisfactory performance gains from 93.8% to 94.1%.

4.2 Part Segmentation

Data Preparation. ShapeNetPart [60] is a popular benchmark dataset for 3D object part segmentation, which provides semantic annotations of 50 different part categories defined on 16 object classes. Following official split, we have 14007 shapes for training and the rest 2874 for testing.

For geometric modeling, we uniformly sampled 2048 spatial points with part labels from given mesh models through PDS. For visual modeling, we expanded the interval of azimuth angles to $\pi/4$ and added another elevation angle of $-\pi/6$, such that $K = 16$, $\theta_k^{az} \in \{k\pi/4\}_{k=1}^8$, $\theta_k^{el} = \{\pm\pi/6\}$, $r = 1$. In the meantime, we generated per-pixel semantic labels on rendered multi-view images as ground truth supervisions of image-based segmentation, where an additional background category is added to the original annotation set.

Architecture of Teacher Branch. In contrast to shape classification/retrieval where there already exist many mature multi-view learning frameworks, there is relatively little effort on image-driven shape segmentation. Hence, we designed a standard single image segmentation architecture as the teacher branch, which is illustrated in Figure. 4. The overall architectural design follows a classic encoder-decoder pipeline (e.g., U-Net [19]) to produce a full-resolution segmentation map. Here, the teacher branch

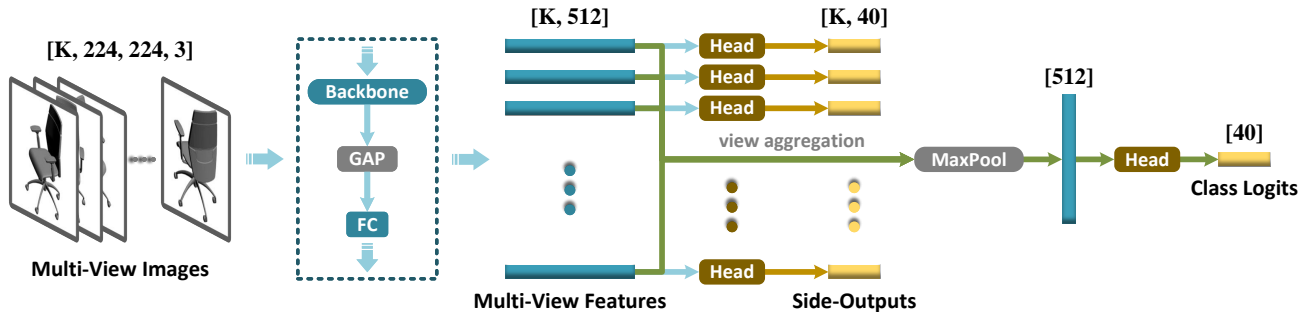


Fig. 3. Teacher learning branch for 2D multi-view image-driven shape classification.

TABLE 1
Overall accuracy (%) of 3D shape classification on ModelNet40.

PointNet		PointNet++		DGCNN		CurveNet	
Original	MV-V2GD	Original	MV-V2GD	Original	MV-V2GD	Original	MV-V2GD
89.2	91.1 (+1.9)	90.7	93.3 (+2.6)	92.9	93.7 (+0.8)	93.8	94.1 (+0.3)

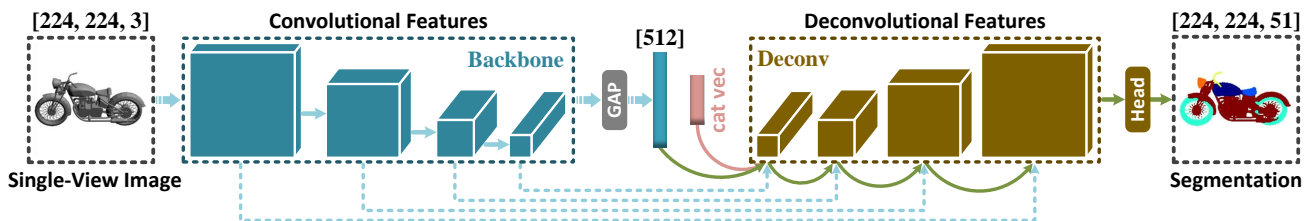


Fig. 4. Teacher learning branch for 2D image-driven object part segmentation.

TABLE 2
Instance-averaged mean intersection-over-union (%) of object part segmentation on ShapeNetPart.

PointNet		PointNet++		DGCNN	
Original	MV-V2GD	Original	MV-V2GD	Original	MV-V2GD
83.7	85.9 (+2.2)	85.1	86.4 (+1.3)	85.1	86.8 (+1.7)

separately consumes a single-view image for prediction, instead of simultaneously segmenting the whole set of multi-view images from the same shape model, since we empirically found that such learning paradigm is computationally-expensive and hard to converge during training.

More specifically, we selected VGG11 [16] as backbone feature extractor and removed the last spatial max-pooling layer to enlarge feature map resolution. To enhance network capacity, we added position and channel attention mechanisms as proposed in [61] into the original convolutional stages, and then fine-tuned the whole backbone network by reconstructing view images rendered from training shapes. Following common practices in previous part segmentation frameworks, we also integrated a categorical vector that encodes object category of the input image into the intermediate visual descriptor.

Architecture of Student Branch. We again adopted PointNet, PointNet++, and DGCNN, as student point encoders \mathcal{M}_s , and employed their original head networks

\mathcal{H}_s to predict per-point semantic labels without voting.

Quantitative results. We listed part segmentation accuracy of both the original and the distilled models in Table 2, from which we can observe that our method consistently enhances different types of deep set architectures. Particularly, PointNet is boosted from 83.7% to 85.9% with large margins in terms of mIoU. The other two more powerful learning frameworks, i.e., PointNet++ and DGCNN, also benefit a lot from MV-V2GD with obvious performance gains of 1.3% and 1.7%, respectively.

4.3 Unsupervised Learning

Previous experiments have demonstrated the effectiveness of MV-V2GD in terms of supervised learning, which requires domain-specific data and annotations. In this section, we explore the possibility of transferring generic 2D visual knowledge acquired by unsupervised feature learning to boost 3D geometric modeling.

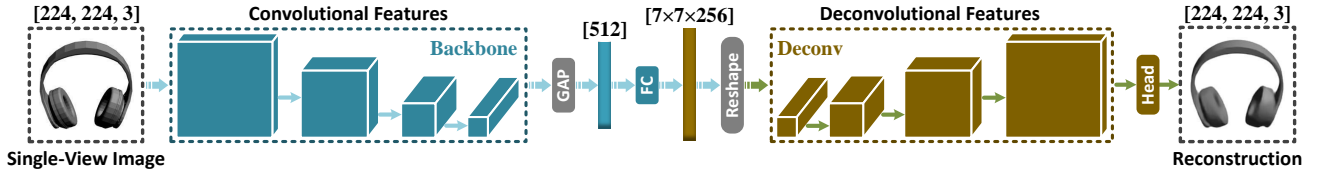


Fig. 5. Teacher learning branch for single-view image reconstruction.

TABLE 3
Transfer classification accuracy (%) on ModelNet40.

Method	Original	MV-V2GD	MV-V2GD (w/o pretraining)
FoldingNet	88.4	89.1 (+0.7)	88.8 (+0.4)

Following the same development protocols (known as *transfer classification*) as constructed in [62], we start by pretraining a deep point cloud auto-encoder on a source dataset (i.e., ShapeNetCoreV2 [63]). After that, we deploy the pretrained encoder network to generate vectorized shape signatures from a different target dataset (i.e., ModelNet40 [7]). Finally, a linear SVM classifier is trained on the target dataset to evaluate the discriminative power of shape signatures.

Data Preparation. ShapeNetCoreV2 [63] is a large-scale 3D object repository containing 52472 polygon mesh models covering 55 object categories.

For geometric modeling, we applied PDS to uniformly sample 2048 spatial points from both ShapeNetCoreV2 and ModelNet40 datasets. For visual modeling, we adopted the same viewpoint configuration as described in Sec. 4.2 to generate multi-view image renderings on ShapeNetCoreV2.

Architecture of Teacher Branch. As illustrated in Figure 5, we constructed a standard convolutional auto-encoder for unsupervised image feature learning. In the encoding phase, we applied the same backbone network as adopted in our part segmentation experiments to compactly represent the input view image as a vectorized shape signature. In the decoding phase, we deployed a fully-connected layer to lift feature dimension as well as several stages of deconvolutional layers to achieve full-resolution image reconstruction.

Architecture of Student Branch. We experimented with a classic point cloud driven unsupervised geometric feature learning architecture, i.e., FoldingNet [62], as the target student branch. Technically, it encodes given points into a compact global codeword vector, which drives the subsequent lattice deformation process for reconstructing the input point cloud.

Quantitative Results. We listed transfer classification accuracy of both the original and the distilled models in Table 3, where we can observe that FoldingNet is boosted from 88.4% to 89.1%.

Besides, we are interested in the potential of transferring common visual cues learned from natural image statistics

without task-specific pretraining. To this end, we directly deployed the original VGG11 backbone network pretrained on ImageNet to provide teacher knowledge, which also enhances the target student model with 0.4% accuracy improvement.

4.4 Additional Explorations

We conducted additional explorations by designing different architecture variants and evaluating their performances on ModelNet40 classification.

Hyperparameter Analysis. To comprehensively explore the characteristics of our learning framework, we modified the original MV-V2GD settings by adjusting two critical hyperparameters: 1) the number of viewpoints K , and 2) the weighting factor ω_t (Eq. 6).

We considered reducing the number of virtual cameras (i.e., K) from 12 to $\{6, 4, 1\}$, which correspond to three model variants, namely: Reduc-6, Reduc-4, and Rand-1. Under the same elevation angle $\theta_k^{el} = \pi/6$ and observation distance $r = 1$, we changed azimuth angles to $\theta_k^{az} \in \{k\pi/3\}_{k=1}^6$ and $\theta_k^{az} \in \{k\pi/2\}_{k=1}^4$ in Reduc-6 and Reduc-4, respectively. For Rand-1, we randomly selected one of the original 12 viewpoints to provide teacher knowledge at each training iteration. As indicated in Table 4, reducing the number of viewpoints inevitably causes performance degradation, due to the loss of visual information captured from those missing views. Note that, although the Rand-1 variant only selects a single random view at each iteration, it basically exploits more different views through the whole training process, and hence shows satisfactory performance.

When formulating the overall training objective $\mathcal{L}_{\text{overall}}$ of MV-V2GD, we searched the optimal weighting scheme by fixing $\omega_d = 1/K$, which is determined uniquely by the number of viewpoints, and experimenting with different values of ω_t , as reported in Table 5. Empirically, combining Table 1 ($\omega_t = 0.1$) and Table 5 ($\omega_t = 0.01, 1.0$), we observed that $\omega_t = 0.1$ turns to be a robust choice that uniformly produces the optimal performance on all three distilled models. Given a smaller $\omega_t = 0.01$, the task loss cannot sufficiently converge, which leads to significant performance degradation. Inversely, a larger $\omega_t = 1.0$ weakens the constraint of the distillation loss, which also

TABLE 4
Influence of different number of rendering viewpoints (K).

PointNet			PointNet++			DGCNN		
Reduc-6	Reduc-4	Rand-1	Reduc-6	Reduc-4	Rand-1	Reduc-6	Reduc-4	Rand-1
91.0	90.8	90.7	93.0	92.9	92.7	93.4	93.2	93.3

TABLE 5
Influence of different weighting schemes (ω_t) in the training objective.

PointNet		PointNet++		DGCNN	
$\omega_t = 0.01$	$\omega_t = 1.0$	$\omega_t = 0.01$	$\omega_t = 1.0$	$\omega_t = 0.01$	$\omega_t = 1.0$
81.9	90.8	83.5	92.9	87.1	93.2

causes sub-optimal results.

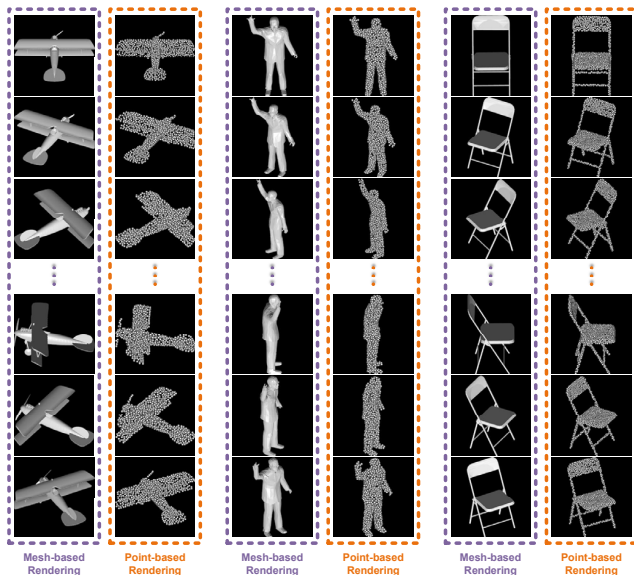


Fig. 6. Visual examples of both mesh-based and point-based rendering results.

Point-based Rendering Pipeline. We attempted to directly render raw point clouds, instead of meshes, into multi-view images for training the teacher branch, which is further deployed to provide visual knowledge for the student branch. Some typical visual examples of point-based rendering as well as their mesh-driven counterparts are shown in Fig. 6. Obviously, such learning strategy is more flexible and practical for applications where high-quality mesh-based geometry representations are unavailable. As reported in Table 6, this variant still shows satisfactory performance boost on all distilled models, which demonstrates the universality of our proposed image-to-point knowledge transfer paradigm.

Training Teacher Models from Scratch. One of the major advantages of the proposed cross-modal (visual-to-geometric) knowledge transfer framework is that we can conveniently exploit mature off-the-shelf visual recognition networks that are sufficiently pretrained on large-scale an-

notated 2D image databases, e.g., ImageNet. A more interesting and promising problem is to explore whether the interaction mechanism between 2D visual and 3D geometric modeling paradigms itself brings benefits. In fact, in our unsupervised learning experiments, we have attempted to verify this problem by training the teacher branch from scratch, which still brings performance gains. Here, we further conducted experiments to strengthen such claims under supervised learning scenarios.

More specifically, we maintained all development protocols unchanged in this point-based rendering experiment, except that we did not load ImageNet pretrained weights for the backbone network of the teacher branch. Quantitative results are shown in Table 7, from which we can *surprisingly* observe that training the teacher branch totally from scratch on point cloud renderings still shows highly competitive performance and even outperforms its ImageNet pretrained and mesh-driven counterpart on PointNet [11]. This phenomenon strongly demonstrates the great potential of the proposed visual-geometric learning paradigms.

Adaptation of Conventional Distillation Paradigms. To reveal the necessity and superiority of our method, we further designed two baseline knowledge transfer pipelines that are directly adapted from classic response-based [53] and feature-based [64] distillation paradigms. The first baseline aims at aligning the final class logits outputted from the last layer of teacher and student branches, which we call Lgt-V2GD. The second baseline is called Ftr-V2GD, which focuses on feature-level guidance by aligning the vectorized global visual and geometric descriptors before feeding them into the subsequent fully-connected classifiers. We listed performance of different baseline frameworks in Table 8, and observed several aspects of consistent trends by combining the corresponding experimental results reported in Table 1.

First, our experimental results strongly reveal that *vision-to-geometry knowledge transfer provides a generic and stable way of enhancing point cloud learning models*. Even the most straightforward distillation framework (Lgt-V2GD) leads to different degrees of performance improvement in all experimental setups. Second, *feature-level teacher guidance tends to be more informative than soft targets (i.e., logits)*, since it is discovered that Ftr-V2GD always outperforms Lgt-V2GD. Third, *the modeling capacity of many existing point*

TABLE 6
Effectiveness of rendering multi-view images from raw point clouds.

PointNet	PointNet++	DGCNN
91.2 (+2.0)	93.0 (+2.3)	93.5 (+0.6)

TABLE 7
Overall accuracy (%) of 3D shape classification on ModelNet40, where teacher models are trained from scratch (i.e., without loading ImageNet pretrained weights).

PointNet		PointNet++		DGCNN	
pretrained	from scratch	pretrained	from scratch	pretrained	from scratch
91.1 (+1.9)	91.5 (+2.3)	93.3 (+2.6)	92.9 (+2.2)	93.7 (+0.8)	93.6 (+0.7)

TABLE 8
Comparison of logit-driven and feature-driven distillation baselines.

PointNet		PointNet++		DGCNN	
Lgt-V2GD	Ftr-V2GD	Lgt-V2GD	Ftr-V2GD	Lgt-V2GD	Ftr-V2GD
90.2	90.4	92.5	92.8	93.0	93.2

cloud learning frameworks may be underestimated, considering the significant performance boost of all the distilled models under our proposed MV-V2GD processing pipeline.

5 DISCUSSION

In this section, we re-emphasize our core motivation and principle when designing the overall processing pipeline as well as new insights brought by our paper, based on which we briefly discuss possible extensions in future efforts.

Ultimately, this paper focuses on revealing the potential of transferring knowledge from 2D visual domain to 3D geometric domain. Hence, we avoid designing complicated learning architectures or strategies throughout the whole workflow, since we believe that concise technical implementations and stable performance gains can strongly demonstrate the value of our method. It can be expected that more advanced multi-view visual-geometric feature alignment techniques as well as distillation objectives will further empower the current MV-V2GD framework.

In terms of experimental setups, we noticed that existing multi-view learning approaches are mainly benchmarked over global geometry modeling tasks, e.g., classification and retrieval, due to the inconvenience of preparing domain-specific datasets, while this work extended the application scenarios to part segmentation and unsupervised learning, forming a more comprehensive evaluation protocol.

More importantly, our encouraging results inspire researchers/developers to pay more attention to data exploitation, in addition to model design. Considering the availability of large-scale richly-annotated 2D visual data and the scarcity of their 3D geometric counterparts, it is a highly promising and economical way of enhancing point cloud learning models through image-to-point distillation.

6 CONCLUSION

In this paper, we made the first attempt to explore the potential of transferring cross-modal knowledge from multi-view 2D visual modeling to 3D geometric modeling for boosting 3D point cloud shape understanding. Technically, we investigated a unified MV-V2GD learning pipeline that applies to common types of deep 3D point cloud-based learning paradigms, and specifically customized a novel VAFP mechanism to achieve heterogeneous feature alignment between multi-view images and point clouds. Extensive experiments on various applications strongly demonstrate the superiority, universality, and stability of our method. We believe that our work will open up new possibilities of developing powerful deep set architectures and motivate more explorations along this promising direction.

REFERENCES

- [1] H. Su, S. Maji, E. Kalogerakis, and E. Learned-Miller, "Multi-view convolutional neural networks for 3d shape recognition," in *Proc. CVPR*, 2015, pp. 945–953. [1](#), [2](#), [5](#)
- [2] E. Kalogerakis, M. Averkiou, S. Maji, and S. Chaudhuri, "3d shape segmentation with projective convolutional networks," in *Proc. CVPR*, 2017, pp. 3779–3788. [1](#)
- [3] T. Yu, J. Meng, and J. Yuan, "Multi-view harmonized bilinear network for 3d object recognition," in *Proc. CVPR*, 2018, pp. 186–194. [1](#), [2](#)
- [4] A. Kanazaki, Y. Matsushita, and Y. Nishida, "Rotationnet: Joint object categorization and pose estimation using multiviews from unsupervised viewpoints," in *Proc. CVPR*, 2018, pp. 5010–5019. [1](#), [2](#)
- [5] X. Wei, R. Yu, and J. Sun, "View-gcn: View-based graph convolutional network for 3d shape analysis," in *Proc. CVPR*, 2020, pp. 1850–1859. [1](#), [2](#)
- [6] D. Maturana and S. Scherer, "Voxnet: A 3d convolutional neural network for real-time object recognition," in *Proc. IROS*, 2015, pp. 922–928. [1](#)
- [7] Z. Wu, S. Song, A. Khosla, F. Yu, L. Zhang, X. Tang, and J. Xiao, "3d shapenets: A deep representation for volumetric shapes," in *Proc. CVPR*, 2015, pp. 1912–1920. [1](#), [5](#), [7](#)

- [8] G. Riegler, A. Osman Ulusoy, and A. Geiger, "Octnet: Learning deep 3d representations at high resolutions," in *Proc. CVPR*, 2017, pp. 3577–3586. **1**
- [9] P.-S. Wang, Y. Liu, Y.-X. Guo, C.-Y. Sun, and X. Tong, "O-cnn: Octree-based convolutional neural networks for 3d shape analysis," *ACM Trans. Graph.*, vol. 36, no. 4, pp. 1–11, 2017. **1**
- [10] R. Klokov and V. Lempitsky, "Escape from cells: Deep kd-networks for the recognition of 3d point cloud models," in *Proc. ICCV*, 2017, pp. 863–872. **1**
- [11] C. R. Qi, H. Su, K. Mo, and L. J. Guibas, "Pointnet: Deep learning on point sets for 3d classification and segmentation," in *Proc. CVPR*, 2017, pp. 652–660. **1, 2, 4, 5, 8**
- [12] C. R. Qi, L. Yi, H. Su, and L. J. Guibas, "Pointnet++: Deep hierarchical feature learning on point sets in a metric space," in *Proc. NeurIPS*, 2017, pp. 5105–5114. **1, 2, 4, 5**
- [13] Y. Li, R. Bu, M. Sun, W. Wu, X. Di, and B. Chen, "Pointcnn: Convolution on χ -transformed points," in *Proc. NeurIPS*, 2018, pp. 828–838. **1, 2**
- [14] H. Thomas, C. R. Qi, J.-E. Deschard, B. Marcotegui, F. Goulette, and L. J. Guibas, "Kpconv: Flexible and deformable convolution for point clouds," in *Proc. ICCV*, 2019, pp. 6411–6420. **1, 2**
- [15] Y. Wang, Y. Sun, Z. Liu, S. E. Sarma, M. M. Bronstein, and J. M. Solomon, "Dynamic graph cnn for learning on point clouds," *ACM Trans. Graph.*, vol. 38, no. 5, pp. 1–12, 2019. **1, 2, 4, 5**
- [16] K. Simonyan and A. Zisserman, "Very deep convolutional networks for large-scale image recognition," in *Proc. ICLR*, 2015. **1, 6**
- [17] K. He, X. Zhang, S. Ren, and J. Sun, "Deep residual learning for image recognition," in *Proc. CVPR*, 2016, pp. 770–778. **1**
- [18] J. Long, E. Shelhamer, and T. Darrell, "Fully convolutional networks for semantic segmentation," in *Proc. CVPR*, 2015, pp. 3431–3440. **1**
- [19] O. Ronneberger, P. Fischer, and T. Brox, "U-net: Convolutional networks for biomedical image segmentation," in *Proc. MICCAI*, 2015, pp. 234–241. **1, 5**
- [20] M. Cordts, M. Omran, S. Ramos, T. Rehfeld, M. Enzweiler, R. Benenson, U. Franke, S. Roth, and B. Schiele, "The cityscapes dataset for semantic urban scene understanding," in *Proc. CVPR*, 2016, pp. 3213–3223. **1**
- [21] M. Everingham, L. Van Gool, C. K. Williams, J. Winn, and A. Zisserman, "The pascal visual object classes (voc) challenge," *IJCV*, vol. 88, no. 2, pp. 303–338, 2010. **1**
- [22] A. Krizhevsky, I. Sutskever, and G. E. Hinton, "Imagenet classification with deep convolutional neural networks," in *Proc. NeurIPS*, vol. 25, 2012, pp. 1097–1105. **1, 3**
- [23] T.-Y. Lin, M. Maire, S. Belongie, J. Hays, P. Perona, D. Ramanan, P. Dollár, and C. L. Zitnick, "Microsoft coco: Common objects in context," in *Proc. ECCV*, 2014, pp. 740–755. **1**
- [24] B. Zhou, H. Zhao, X. Puig, T. Xiao, S. Fidler, A. Barriuso, and A. Torralba, "Semantic understanding of scenes through the ade20k dataset," *IJCV*, vol. 127, no. 3, pp. 302–321, 2019. **1**
- [25] S. Tulsiani, A. A. Efros, and J. Malik, "Multi-view consistency as supervisory signal for learning shape and pose prediction," in *Proc. CVPR*, 2018, pp. 2897–2905. **1**
- [26] X. He, Y. Zhou, Z. Zhou, S. Bai, and X. Bai, "Triplet-center loss for multi-view 3d object retrieval," in *Proc. CVPR*, 2018, pp. 1945–1954. **1**
- [27] Y. Feng, Z. Zhang, X. Zhao, R. Ji, and Y. Gao, "Gvcnn: Group-view convolutional neural networks for 3d shape recognition," in *Proc. CVPR*, 2018, pp. 264–272. **2**
- [28] Z. Yang and L. Wang, "Learning relationships for multi-view 3d object recognition," in *Proc. ICCV*, 2019, pp. 7505–7514. **2**
- [29] C. Esteves, Y. Xu, C. Allen-Blanchette, and K. Daniilidis, "Equivariant multi-view networks," in *Proc. ICCV*, 2019, pp. 1568–1577. **2**
- [30] A. Hamdi, S. Giancola, and B. Ghanem, "Mvtn: Multi-view transformation network for 3d shape recognition," in *Proc. ICCV*, 2021, pp. 1–11. **2**
- [31] B.-S. Hua, M.-K. Tran, and S.-K. Yeung, "Pointwise convolutional neural networks," in *Proc. CVPR*, 2018, pp. 984–993. **2, 4**
- [32] N. Verma, E. Boyer, and J. Verbeek, "Feastnet: Feature-steered graph convolutions for 3d shape analysis," in *Proc. CVPR*, 2018, pp. 2598–2606. **2**
- [33] M. Xu, R. Ding, H. Zhao, and X. Qi, "Paconv: Position adaptive convolution with dynamic kernel assembling on point clouds," in *Proc. CVPR*, 2021, pp. 3173–3182. **2, 5**
- [34] J. Li, B. M. Chen, and G. H. Lee, "So-net: Self-organizing network for point cloud analysis," in *Proc. CVPR*, 2018, pp. 9397–9406. **2, 4**
- [35] H. Su, V. Jampani, D. Sun, S. Maji, E. Kalogerakis, M.-H. Yang, and J. Kautz, "Splatnet: Sparse lattice networks for point cloud processing," in *Proc. CVPR*, 2018, pp. 2530–2539. **2**
- [36] Y. Liu, B. Fan, S. Xiang, and C. Pan, "Relation-shape convolutional neural network for point cloud analysis," in *Proc. CVPR*, 2019, pp. 8895–8904. **2, 4, 5**
- [37] W. Wu, Z. Qi, and L. Fuxin, "Pointconv: Deep convolutional networks on 3d point clouds," in *Proc. CVPR*, 2019, pp. 9621–9630. **2**
- [38] Z. Zhang, B.-S. Hua, and S.-K. Yeung, "Shellnet: Efficient point cloud convolutional neural networks using concentric shells statistics," in *Proc. ICCV*, 2019, pp. 1607–1616. **2, 4**
- [39] J. Yang, Q. Zhang, B. Ni, L. Li, J. Liu, M. Zhou, and Q. Tian, "Modeling point clouds with self-attention and gumbel subset sampling," in *Proc. CVPR*, 2019, pp. 3323–3332. **2**
- [40] E. Nezhadarya, E. Taghavi, R. Razani, B. Liu, and J. Luo, "Adaptive hierarchical down-sampling for point cloud classification," in *Proc. CVPR*, 2020, pp. 12956–12964. **2, 4**
- [41] X. Yan, C. Zheng, Z. Li, S. Wang, and S. Cui, "Pointasnl: Robust point clouds processing using nonlocal neural networks with adaptive sampling," in *Proc. CVPR*, 2020, pp. 5589–5598. **2, 4**
- [42] M.-H. Guo, J.-X. Cai, Z.-N. Liu, T.-J. Mu, R. R. Martin, and S.-M. Hu, "Pct: Point cloud transformer," *Computational Visual Media*, vol. 7, no. 2, pp. 187–199, 2021. **2**
- [43] H. Zhao, L. Jiang, J. Jia, P. H. Torr, and V. Koltun, "Point transformer," in *Proc. ICCV*, 2021, pp. 16 259–16 268. **2**
- [44] H. Fan, Y. Yang, and M. Kankanhalli, "Point 4d transformer networks for spatio-temporal modeling in point cloud videos," in *Proc. CVPR*, 2021, pp. 14 204–14 213. **2**
- [45] L. Hui, H. Yang, M. Cheng, J. Xie, and J. Yang, "Pyramid point cloud transformer for large-scale place recognition," in *Proc. ICCV*, 2021, pp. 6098–6107. **2**
- [46] P. Xiang, X. Wen, Y.-S. Liu, Y.-P. Cao, P. Wan, W. Zheng, and Z. Han, "Snowflakenet: Point cloud completion by snowflake point deconvolution with skip-transformer," in *Proc. ICCV*, 2021, pp. 5499–5509. **2**
- [47] K. Mazur and V. Lempitsky, "Cloud transformers: A universal approach to point cloud processing tasks," in *Proc. ICCV*, 2021, pp. 10 715–10 724. **2**
- [48] J. Gou, B. Yu, S. J. Maybank, and D. Tao, "Knowledge distillation: A survey," *International Journal of Computer Vision*, vol. 129, no. 6, pp. 1789–1819, 2021. **2**
- [49] M. Jaritz, T.-H. Vu, R. d. Charette, E. Wirbel, and P. Pérez, "xmuda: Cross-modal unsupervised domain adaptation for 3d semantic segmentation," in *Proc. CVPR*, 2020, pp. 12 605–12 614. **3**
- [50] Y.-C. Liu, Y.-K. Huang, H.-Y. Chiang, H.-T. Su, Z.-Y. Liu, C.-T. Chen, C.-Y. Tseng, and W. H. Hsu, "Learning from 2d: Pixel-to-point knowledge transfer for 3d pretraining," *arXiv preprint arXiv:2104.04687*, 2021. **3**
- [51] J. Hou, S. Xie, B. Graham, A. Dai, and M. Nießner, "Pri3d: Can 3d priors help 2d representation learning?" in *Proc. ICCV*, 2021, pp. 5693–5702. **3**
- [52] Z. Liu, X. Qi, and C.-W. Fu, "3d-to-2d distillation for indoor scene parsing," in *Proc. CVPR*, 2021, pp. 4464–4474. **3**
- [53] G. Hinton, O. Vinyals, and J. Dean, "Distilling the knowledge in a neural network," *arXiv preprint arXiv:1503.02531*, 2015. **3, 8**
- [54] M. Lin, Q. Chen, and S. Yan, "Network in network," in *Proc. ICLR*, 2014. **3**
- [55] S. Katz, A. Tal, and R. Basri, "Direct visibility of point sets," in *ACM SIGGRAPH*, 2007, pp. 24–es. **4**
- [56] J.-C. Su, M. Gadelha, R. Wang, and S. Maji, "A deeper look at 3d shape classifiers," in *Proceedings of the European Conference on Computer Vision (ECCV) Workshops*, 2018, pp. 0–0. **5**
- [57] M. Sandler, A. Howard, M. Zhu, A. Zhmoginov, and L.-C. Chen, "Mobilenetv2: Inverted residuals and linear bottlenecks," in *Proc. CVPR*, 2018, pp. 4510–4520. **5**
- [58] T. Xiang, C. Zhang, Y. Song, J. Yu, and W. Cai, "Walk in the cloud: Learning curves for point clouds shape analysis," pp. 915–924, 2021. **5**
- [59] Z. Liu, H. Hu, Y. Cao, Z. Zhang, and X. Tong, "A closer look at local aggregation operators in point cloud analysis," in *Proc. ECCV*, 2020, pp. 326–342. **5**
- [60] L. Yi, V. G. Kim, D. Ceylan, I.-C. Shen, M. Yan, H. Su, C. Lu, Q. Huang, A. Sheffer, and L. Guibas, "A scalable active framework

- for region annotation in 3d shape collections," *ACM Trans. Graph.*, vol. 35, no. 6, pp. 1–12, 2016. [5](#)
- [61] J. Fu, J. Liu, H. Tian, Y. Li, Y. Bao, Z. Fang, and H. Lu, "Dual attention network for scene segmentation," in *Proc. CVPR*, 2019, pp. 3146–3154. [6](#)
- [62] Y. Yang, C. Feng, Y. Shen, and D. Tian, "Foldingnet: Point cloud auto-encoder via deep grid deformation," in *Proc. CVPR*, 2018, pp. 206–215. [7](#)
- [63] A. X. Chang, T. Funkhouser, L. Guibas, P. Hanrahan, Q. Huang, Z. Li, S. Savarese, M. Savva, S. Song, H. Su *et al.*, "Shapenet: An information-rich 3d model repository," *arXiv preprint arXiv:1512.03012*, 2015. [7](#)
- [64] A. Romero, N. Ballas, S. E. Kahou, A. Chassang, C. Gatta, and Y. Bengio, "Fitnets: Hints for thin deep nets," in *Proc. ICLR*, 2015. [8](#)